Recombination of photodissociated iodine: A time-resolved x-ray-diffraction study

M. Wulff
European Synchrotron Radiation Facility, Grenoble Cedex 38043, BP 220, France

S. Bratos[a)]
Laboratoire de Physique, Théorique des Liquides, Université Pierre et Marie Curie, Case Courrier 121, 4 Place Jussieu, Paris Cedex 75252, France

A. Plech
Fachbereich Physik der Universität Konstanz, Universitätsstrasse 10, D-78457 Konstanz, Germany

R. Vuilleumier and F. Mirloup
Laboratoire de Physique, Théorique des Liquides, Université Pierre et Marie Curie, Case Courrier 121, 4 Place Jussieu, Paris Cedex 75252, France

M. Lorenc and Q. Kong
European Synchrotron Radiation Facility, Grenoble Cedex 38043, BP 220, France

H. Ihee
Department of Chemistry, Korea Advanced Institute of Science and Technology, Daejeon 305-701, Korea and School of Molecular Science (BK21), Korea Advanced Institute of Science and Technology, Daejeon 305-701, Korea

(Received 6 October 2005; accepted 11 November 2005; published online 17 January 2006)

A time-resolved x-ray-diffraction experiment is presented that aims to study the recombination of laser-dissociated iodine molecules dissolved in CCl_4. This process is monitored over an extended time interval from pico- to microseconds. The variations of atom-atom distances are probed with a milliangstrom resolution. A recent theory of time-resolved x-ray diffraction is used to analyze the experimental data; it employs the correlation function approach of statistical mechanics. The most striking outcome of this study is the experimental determination of time-dependent I–I atom-atom distribution functions. The structure of the CCl_4 solvent changes simultaneously; the solvent thus appears as a reaction partner rather than an inert medium hosting it. Thermal expansion of the system is nonuniform in time, an effect due to the presence of the acoustic horizon. One concludes that a time-resolved x-ray diffraction permits real-time visualization of solvent and solute motions during a chemical reaction. © *2006 American Institute of Physics*. [DOI: 10.1063/1.2149852]

I. INTRODUCTION

The iodine photodissociation and recombination in solutions has been studied for 70 years as a prototype of a simple chemical reaction. Franck and Rabinowitch suggested in 1934 that the solvents may trap the initial atom pair from a photodissociated molecule, and force the two atoms to recombine in a cage in the solvent.[1–3] Noyes and co-workers carried out quantitative studies of the recombination rates as a function of the solvent viscosity and the wavelength of the incident light 20 year later.[4,5] Detailed studies of atom recombination in the gas phase have also been done. Moreover, the density dependence of recombination yields has been investigated in fluids across the density range from gases to liquids.

A new chapter was opened in 1970's–1980's when Mulliken realized his remarkable quantum-chemical calculations of the electronic structure of the iodine molecule.[6] A few years later, Chuang *et al.*,[7] Harris *et al.*,[8] Abul-Haj and Kelley,[9] and Harris *et al.*[10] published beautiful laser-spectroscopic studies in which the photodissociation and recombination processes were monitored in real time. This effort was completed by molecular-dynamics simulations realized by Bergsma *et al.*[11] Combining experimental and theoretical data then provided a much better understanding of microscopic dynamics. However, the reaction was found to be far more complex than believed initially. Characteristic time scales of these processes were determined with great care.

The third and newest era in studying this problem was initiated by the advent of ultrafast x-ray diffraction and absorption.[12–18] The reaction is still triggered optically, but the recombination is probed by diffraction of ultrashort x-ray pulses. Their wavelength is typically of the order of 1 A, which permits to track the motions of individual atoms. The difficulty is that the time-resolved x-ray diffraction is a very demanding method both experimentally and theoretically. However, an early experimental study of a I_2/CH_2Cl_2 solution proved its feasibility.[19] The basic theory was elaborated at about the same time.[20,21]

The purpose of this paper is to present a detailed account of our recent time-resolved x-ray-diffraction study of the re-

[a)]Electronic mail: bratos@lptl.jussieu.fr

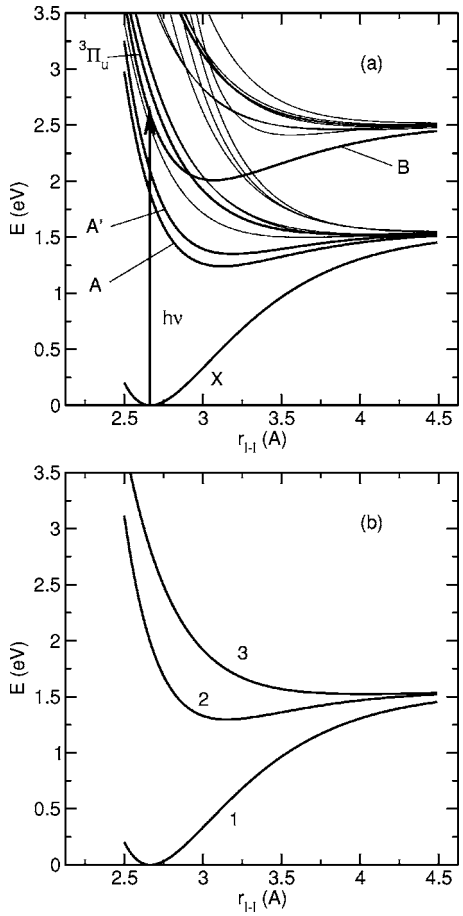

FIG. 1. (a) Electronic energy surfaces of the I_2 molecule. The states X, A, A', and B are attractive, whereas the others are repulsive. (b) Electronic energy surfaces of the model: state 1 corresponds to the molecular state X, state 2 to the molecular states A, A', and state 3 represents a collection of repulsive molecular states.

combination of laser-dissociated I_2 in CCl_4. Preliminary results have been published elsewhere.[22,23] However, as these techniques are very new, an *in extenso* systematic presentation of this work seems to be useful. The main novelty of our work is the experimental determination of temporally varying I–I and Cl–Cl atom-atom distribution functions. The solvent participates in the reaction. It appears as a reaction partner rather than an inert medium. Affected by the presence of an acoustic horizon, thermal expansion is not uniform in time. One concludes that the pulsed x-ray diffraction permits a visualization in real time of solvent and solute motions during a chemical reaction.

II. EXPERIMENT

A. Basic principles

The system to be studied is a dilute I_2/CCl_4 solution. This solution is pumped by an optical laser, which promotes the iodine molecule into its excited electronic states [Fig. 1(a)]. The states X, A, A', and B are attractive, and the state $^1\pi_u$ is repulsive. The iodine molecule explodes and dissociates into a pair of nonbonded atoms. Two outcomes are then possible. The solvent can trap the atoms and force them to recombine in a process called geminate recombination. Alternatively, they may escape the solvent cage and recombine with other partners; this is a nongeminate recombination. Time-delayed x-ray diffraction is used to probe the recombination.

This rough picture can be sharpened by the following information. The excitation of an I_2 molecule generates a mixture of the electronic states B and $^1\pi_u$, which mainly dissociate into ground-state atoms. A hot iodine molecule, $I_2^\star$ molecule, is then formed in less than 1 ps. Its bond length R, of the order of 4 A, is only vaguely defined. The subsequent recombination is most often geminate. The process $I_2^\star \Rightarrow I_2$ can be realized either directly by vibrational cooling, or indirectly by passing through the bound states A/A'. The recombination may also be nongeminate. It involves the escape $I_2^\star \Rightarrow 2I$ of an iodine atom from the cage, and its recombination $2I \Rightarrow I_2$ with some other iodine atom in solution. Three times govern these processes, called α, β, and γ.[7–10] The time $\tau_\alpha = 0.18$ ns is associated with the relaxation of hot $I_2^\star$ along the X state potential; the time $\tau_\beta = 2.7$ ns is ascribed to the relaxation of the A/A' state populations; and the time $\tau_\gamma \sim 25$ ns describes the nongeminate recombination.

The experimental setup is illustrated in Fig. 2. It comprises a pulsed synchrotron source, a chopper that selects single x-ray pulses, a femtosecond laser, a capillar jet, and an integrating charge-coupled device (CCD) detector.[24,25] An undulator formed by an array of alternating magnets was placed inside the vacuum vessel of the synchrotron to increase the intensity of the diffracted beam. A gain in intensity by a factor of 2–4 is obtainable in this way. The images were integrated azimuthally and corrected for polarization and space-angle effects. These precautions are all necessary, the signal from the solute being very small as compared to the signal from the solvent. The above experiments were realized on beamline ID09B at the ESRF in Grenoble. The setup will now be described in some detail, from the synchrotron to the software used to reduce the data.

B. Sources of x-ray radiation

The x-rays were produced by a 236 pole in-vacuum undulator with a magnetic period of 17 mm. The undulator was operated at 10.5 mm gap where its SmCo magnets produced an oscillatory magnetic field with an amplitude of 0.24 T. The energy of the electrons was 6.03 GeV, which corresponds to a relativistic parameter $\gamma = [1-(v^2/c^2)]^{-1/2} = 11\,800$. At this gap the undulator spectrum is dominated by its first harmonic, which peaks at 19.0 kev ($\lambda = 0.652$ A). The width of the triangularly shaped spectrum was $d\lambda/\lambda = 0.03$ (Fig. 3). Each pulse delivered 3.8×10^8 photons on the sample, and its duration varied between 145 and 175 ps [full width at half maximum (FWHM)]. The x rays were 99.4% polarized in the horizontal plane. Considering the spectrum of the undulator and the mirror reflectivity, the intensity of higher harmonics was estimated to be smaller than 2%. A torroidal mirror condensed the beam into a 0.1-mm-diam spot. It was further reduced by a slit with a square aperture of 0.06×0.06 mm^2. The synchrotron was operated in single-bunch mode, and the ring current varied between 10 and 15 mA. The bunches of electrons rotate around the

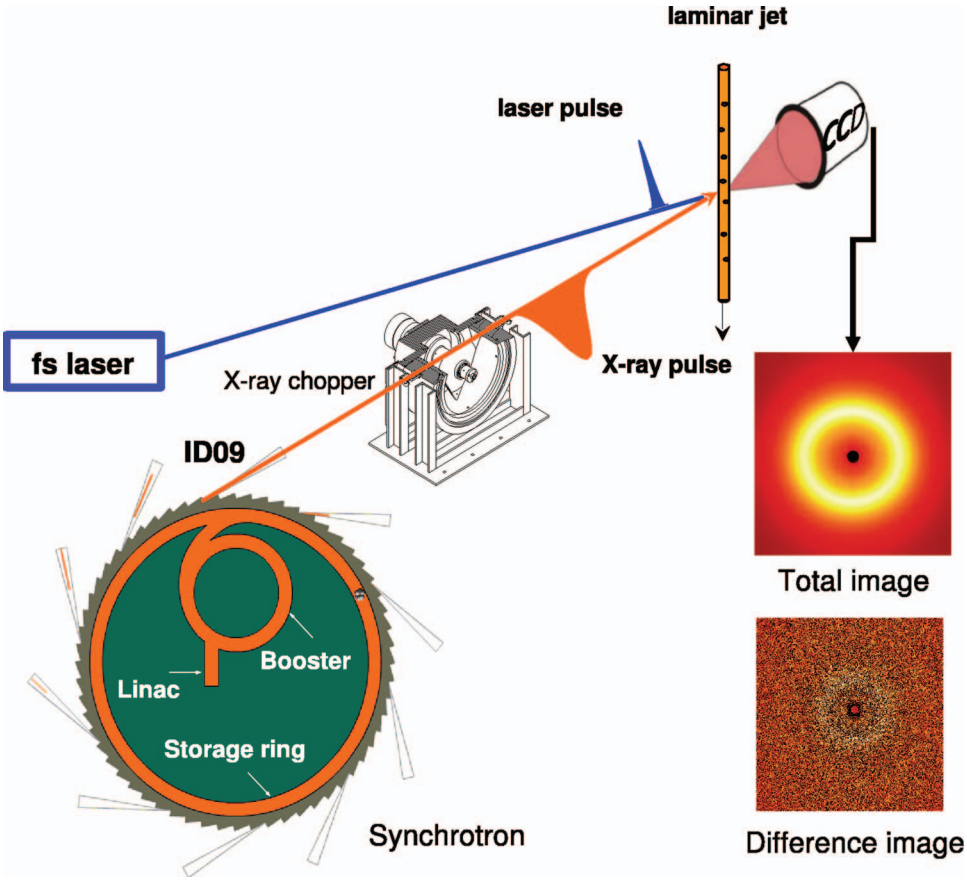

FIG. 2. (Color) Schematic view of the experimental setup. The x-ray pulses are generated by a synchrotron and are interrupted by a chopper. The other important elements of the setup comprise the femtosecond Ti-sapphire laser and the CCD detector.

844-m-long ring in 2.82 μs, which corresponds to an x-ray frequency of 355.0 kHz. In practice it is impossible to run pump-probe experiments at this frequency, and a chopper was used to isolate a subtrain of pulses at 896.6 Hz; this frequency is the 396th subharmonic of the orbit frequency.

C. Sources of optical radiation

The sample was excited by a 520 nm laser beam. This beam was generated by a femtosecond optical parametric amplifier (OPA), pumped by a Ti:sapphire oscillator. The laser-pulse duration was 150 fs and its energy 33 μJ. The laser was running at 896.9 Hz in phase with the chopper. The beam was focused on the sample to a diameter of 0.12 mm, and the corresponding power density peaked at 20 GW/mm^2. The time difference between the two pulse trains was controlled electronically by shifting the phase of the oscillator feedback loop with a digital delay generator with 2.5 ps resolution. Larger delays were realized by amplifying a different oscillator pulse of the 80.05 MHz pulse train. The short-time jitter in the delay was typically 3 ps. At longer times, however, the decay in the bunch charge led to a systematic shift, which may have been as great as 50 ps. The light beam was directed towards the sample with a 10° tilt to the x-ray beam.

The I_2 molecules were dissolved in CCl_4 at a concentration $c=29\times10^{-3}$ mol/liter, or with $N_{I_2}/N_{CCl_4}=1/357$. This corresponds to an average I_2–I_2 distance of 38.5 A, sufficiently dilute to avoid aggregation. The solution was flowed across a 0.3-mm-thick capillary at a speed of 0.1 m/s, fast enough to separate the laser-heated portions of the flowing liquid in the 896.6 Hz beam. The molar extinction coefficient for I_2 in the gas phase is $\varepsilon=81\times10^3$ liter/(mol m) at 520 nm; for a 0.3 mm sample the optical density was 0.70. If Lambert-Beer's law is applied literally, omitting nonlinear effects such as two-photon absorption, one finds that 80% of the incoming laser photons are absorbed by I_2 in the sample. This order of magnitude is believed to remain correct even if nonlinear effects are considered.

D. Charge-coupled device (CCD)

The CCD is an integrating detector without time resolution. The scattered x rays were recorded on a 133-mm-diam

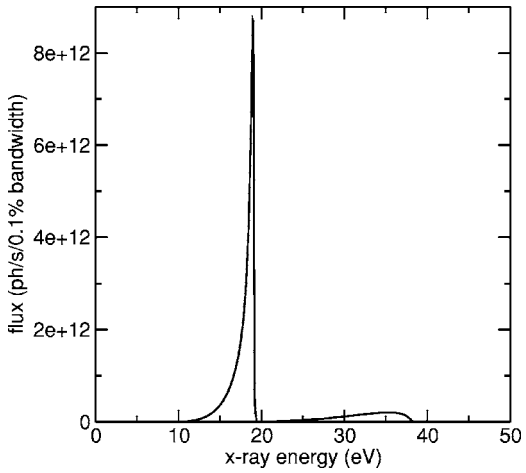

FIG. 3. Spectral shape of an x-ray pulse generated by the U17 undulator. The synchrotron was operating in single bunch mode at 10 mA.

MarCCD detector placed downstream the sample at a distance of 45 mm. This allowed to probe an angular range from 2.9° to 56.0°. The CCD chip was based on a matrix with 2048×2048 pixels, which is subdivided into four 1024×1024 CCD's that are readout in parallel at 16 bits. The time needed for readout, image correction, and saving was 7.6 s. The scattered x rays were first converted into optical light on a 0.040-mm-thick phosphor screen, and the image was then relayed onto the CCD via taper optics with a demagnification of 46%. The circular image is inscribed on the square CCD which lead to an effective pixel size of 64.276 μm. The point-spread function (PSF) was 155 μm. The quantum efficiency at 19 keV was 52%, and the gain in the conversion of x rays to CCD counts was 1.0 analog digital units (ADU) per absorbed x-ray photon at 19 keV. The CCD was kept in vacuum and cooled to −70 °C to reduce the dark current to about 0.02 ADU/s. The readout noise was 0.1 ADU/pixel. The exposure time was 5 s/image. To keep the x-ray dose constant during the data collection, the exposure time was prolonged to compensate for the decaying synchrotron current. This precaution is important. If the exposure time was kept constant, the nonlinearity of the CCD would produce its own difference signal. The data collection protocol was worked out to minimize the effect of drifts (beam motions, detector drifts, sample drifts, etc.). In practice, the best difference images were obtained when the nonexcited and excited states were recorded in the sequence nonexcited, excited, nonexcited, and so on. The nonexcited image was chosen at a negative time delay of −3 ns, to keep the temperature of the capillary constant. Proceeding as described, 36 delays between −150 ps and 1 μs were recorded with a nominal exposure time of 5.0 s. Each time sequence was repeated five times.

E. Data-reducing routines

The CCD images were read by a processing software FIT2D,[26] and the position of the incident beam was determined from the CCl_4 liquid peak at $2\theta = 7.6$, where 2θ is the diffraction angle. Parasitic counts from radioactivity in the taper optics and cosmic rays were eliminated by subtracting two images, the original minus the 180 rotated. In fact, as the incident x-ray radiation was polarized horizontally, the distribution of scattering events should be symmetric with respect to this mirror plane as well as to a twofold rotation axis directed along the beam. Pixels with a difference exceeding ±500 ADU were masked. Finally, the cleaned images were radially integrated and corrected for polarization and geometrical effects.

An important difficulty in the experiment is that each CCD image contains contributions, not only from the solute, but also from the solvent, capillary, and air. The detector noise is omnipresent and complicates the analysis (Fig. 4). A comparison of a raw and a difference signal measured at 450 ps shows spectacularly the size of this effect (Fig. 5): the latter is typically 1000 times weaker than the former! *Ad hoc* methods were employed to minimize the disturbing effects of statistical noise and drifts. One of them consists in normalizing the total signal to 1 at $2\theta = 44$ ($q = 7.07$ A), which

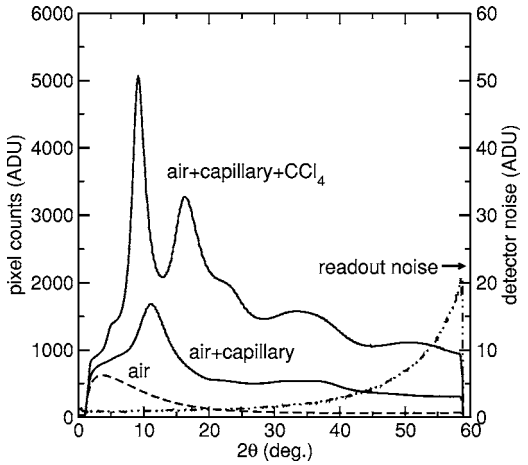

FIG. 4. Contributions to the scattered x-ray intensity on the CCD detector.

forces the difference signals to cross zero at this angle. This point was chosen judiciously to have a minimum effect on the measured difference in zero crossings in gas-phase transitions for iodine. Note that the noise in the difference signal originates almost entirely from the photon statistics from the solvent background.

The difference curves can be put on absolute scale by scaling it to the nonexcited solvent/solute background. At high angles the scattering pattern can be considered as arising from a collection of noninteracting gas molecules rather than from a liquid solution. The Compton scattering cannot be neglected, but it is independent of molecular structure. In this way the concentration of excited molecules can be determined. Another problem is that the incident x-ray radiation is not strictly monochromatic (Fig. 3). This problem may be handled in different ways, e.g., by approximating its spectral distribution by its first spectral moment.[25] The theory developed below includes this effect automatically.

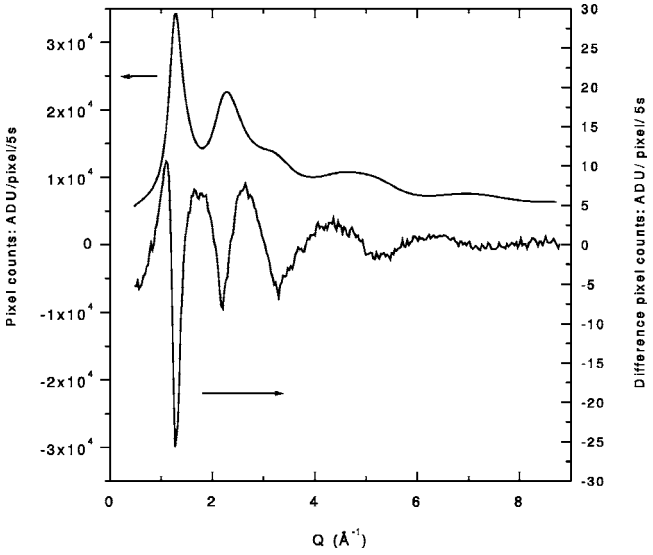

FIG. 5. The total signal $S(q,\tau)$ (top) and the difference signal $\Delta S(q,\tau)$ (bottom). The former is scaled on the left and the latter on the right.

III. THEORY

A. General expression for diffracted signal

The system under consideration is a spatially isotropic liquid. It is submitted to an intense optical pulse of frequency Ω which triggers the process to be investigated τ seconds later, an x-ray pulse is diffracted by it. The time evolution of the system is monitored in this way. The measured quantity is the difference signal $\Delta S(\mathbf{q},\tau)$, defined as the time-integrated x-ray energy flux $S(\mathbf{q},\tau)$ scattered in a given solid angle in presence of the pump, minus the time-integrated x-ray energy flux $S(\mathbf{q})$ in the same solid angle in the absence of the pump. It depends on two variables: the scattering wave vector $\mathbf{q}=\mathbf{q}_I-\mathbf{q}_S$, where $\mathbf{q}_I$ and $\mathbf{q}_S$ are wave vectors of the incident and the scattered x-ray radiation, respectively, and the time delay τ between pump and probe.

The recently published theory of time-resolved x-ray diffraction involves two steps.[21,23] The first consists in developing a Maxwell-type theory of x-ray scattering by an optically excited system of charges and currents. In the second step these currents, that are supposed to be known in the first step, are actually calculated. Methods of statistical mechanics of nonlinear optical processes are employed to achieve this goal. It was then found that the difference signal $\Delta S(\mathbf{q},\tau)$ appears as a convolution between the temporal profile of the x-ray pulse envelope $I_X(t)$ and the diffraction signal of an infinitely sharp x-ray pulse $\Delta S_{\mathrm{inst}}(\mathbf{q},t)$. The result is

$$\Delta S(\mathbf{q},\tau)=\int_{-\infty}^{\infty} dt I_X(t-\tau)\Delta S_{\mathrm{inst}}(\mathbf{q},t),$$

$$\begin{aligned}\Delta S_{\mathrm{inst}}(\mathbf{q},t)=&-\left(\frac{e^2}{mc^2\hbar}\right)^2 P\int_{-\infty}^{\infty}\int_{-\infty}^{\infty} d\tau_1 d\tau_2\\ &\times\langle E_i(\mathbf{r},t-\tau_1)E_j(\mathbf{r},t-\tau_1-\tau_2)\rangle_O\\ &\times\langle[[f(\mathbf{q},\tau_1+\tau_2)f^{\star}(\mathbf{q},\tau_1\\ &+\tau_2),M_i(\tau_2)],M_j(0)]\rangle_S,\end{aligned} \tag{1}$$

where $\mathbf{E}=(E_x,E_y,E_z)$ is the electric field of the optical pulse, $\mathbf{M}=(M_x,M_y,M_z)$ the dipole moment of the system, and $f(\mathbf{q},\tau)=\int d\mathbf{r}e^{i\mathbf{qr}}\rho(\mathbf{r},\tau)$ is the Fourier-transformed electron density. The indices i,j designate the Cartesian components x,y,z of the vectors $\mathbf{E}$, $\mathbf{M}$ and P is the polarization factor. The average $\langle\cdots\rangle_{\mathrm{O}}$ is over all possible realizations of the optical pulse, and the average $\langle\cdots\rangle_{\mathrm{S}}$ is over the states of the nonperturbed molecular system. Two three-time correlation functions are present in Eq. (1): the correlation function of $\mathbf{E}(\mathbf{r},t)$ and the correlation function of the variables $f(\mathbf{q},t),\mathbf{M}(t)$. Such objects are typical for statistical mechanics of systems out of equilibrium, and are well known in time-resolved optical spectroscopy.

It is worth noting that the above expression for $\Delta S(\mathbf{q},\tau)$ depends on the properties of the material system and of the laser fields. They determine jointly the form of the signal. Material properties of the system are accounted for by the correlation function of the variables $f(\mathbf{q},t),\mathbf{M}(t)$, whereas the characteristics of the laser fields are described by the correlation function of the electric field $\mathbf{E}(\mathbf{r},t)$. The signal is nonvanishing even at small negative times, which is due to the overlap between the pump and probe pulses. Equation (1) is an exact second-order perturbation theory result. It is valid at short and long times and applies to a variety of situations. The system may be chemically inert or reactive. However, the laser perturbation should not be too strong if the perturbation series is to be truncated after its second-order term. This approach will now be used to study the recombination of iodine.

B. Quasistatic limit

The theory described above has a comparatively simple limit if the optical excitation is fast as compared with the chemical reaction. This so-called quasistatic condition is of great practical importance. In fact, optical pumping is generally done on the subpicosecond time scale, whereas with present state of the art, the x-ray probing is at least 100 times longer. The simplicity of this situation is due to the fact that, if two dynamic variables evolve on vastly different time scales, they are essentially independent. In the present context, the slow variable is the reaction-driven electron density f, and the fast variable is the laser controlled dipole moment M. The correlation function $\langle[[ff^{\star},M],M]\rangle$ in Eq. (1) thus splits into two factors, a factor involving $f,f^{\star}$ and a factor involving M,M. A quasistatic experiment thus has the intrinsic power to disentangle these two sorts of dynamics. This is the first simplification in this problem.

A second simplification results from introducing the Born-Oppenheimer separation of electronic and nuclear motions; for convenience, the latter will be considered to be classical. Each excited electronic state of the molecule can then be considered as a distinct molecular species, and the laser-excited system can be viewed as a mixture of them. The local structure of such a system is generally described in terms of atom-atom distribution functions $g_{\mu\nu}(r,t)$. These functions are proportional to the probability of finding the nuclei of atoms μ and ν at the distance r at time t. Building this information into Eq. (1) and considering the isotropy of a liquid system, the following result is obtained:

$$\Delta S(q,\tau)=\int_{-\infty}^{\infty} dt I_X(t-\tau)\Delta S_{\mathrm{inst}}(q,t),$$

$$\begin{aligned}\Delta S_{\mathrm{inst}}(q,t)=&\left(\frac{e^2}{mc^2}\right)^2 P\left\{\sum_{\mu\neq}\sum_{\nu} f_\mu f_\nu\left[\frac{1}{V(t)}\int_0^{\infty} dr'\right.\right.\\ &\times 4\pi r'^2(g_{\mu\nu}(r',t)-1)\frac{\sin qr'}{qr'}-\frac{1}{V(0)}\\ &\left.\left.\times\int_0^{\infty} dr' 4\pi r'^2(g^0_{\mu\nu}(r')-1)\frac{\sin qr'}{qr'}\right]\right\}.\end{aligned} \tag{2}$$

This is the quasistatic signal $\Delta S(q,\tau)$ which was desired. In this expression $g_{\mu\nu}(r',t)$ and $g^0_{\mu\nu}(r')$ are the atom-atom distribution functions before and after laser excitation, $f_\mu(q)$ and $f_\nu(q)$ are atomic form factors, and $V(t)$ is the volume of the system. The sums Σ_μ,Σ_ν extend over all pairs of nuclei. Note that the functions $g_{\mu\nu}(r',t)$ are averaged over all laser-

excited electronic states j, carrying the populations $n_j(t)$. Then, if the $g^j_{\mu\nu}(r',\tau)$'s describe atom-atom distributions in the electronic state j, one finds

$$g_{\mu\nu}(r',t) = \sum_j n_j(t) g^j_{\mu\nu}(r',t). \tag{3}$$

IV. VISUALIZATION OF ATOMIC MOTIONS

A. Fourier-transformed signals $\Delta S[r,\tau]$

Once the basic theory of time-resolved x-ray diffraction is established, the problem of visualization of atomic motions can be tackled. As widely known, "photographing" atomic positions in a liquid can be achieved in static problems by Fourier transforming the x-ray-diffraction pattern.[27–29] The situation is particularly simple for atomic liquids, where the well-known Zernicke-Prins formula provides $g(r)$ directly.[27] Can this technique be used, mutatis mutandis, to "film" atomic motions in real time? A convenient starting point in this study consists in introducing a properly normalized Fourier sine transform of the quantity $M(q)q\Delta S(q,\tau)$, where M is the normalization factor $M(q) = [\Sigma_{\mu\neq\nu} f_\mu(q) f_\nu(q)]^{-1}$. Then, by definition

$$\Delta S[r,\tau] = \frac{1}{2\pi^2 r}\int_0^\infty dq \left[\sum_{\mu\neq}\sum_\nu f_\mu(q) f_\nu(q)\right]^{-1} \times q\Delta S(q,\tau)\sin(qr). \tag{4}$$

This signal $\Delta S[r,\tau]$ has to be evaluated for a large number of distances r and a large number of times τ. But before doing that, its physical meaning must be clearly understood. Can it really provide information about molecular motions in liquids? If so, in what way? Are there complications inherent in this approach?

To clarify these questions, the quasistatic signal $\Delta S(q,\tau)$ in Eq. (2) will be substituted into its Fourier transform $\Delta S[r,\tau]$ in Eq. (4). The hope is that one can find an expression that permits a physical interpretation. This happens to be the case. In fact, using this approach the following expression for $\Delta S[r,\tau]$ is obtained

$$\Delta S[r,\tau] = \int_{-\infty}^\infty dt I_X(t-\tau)\Delta S_{\text{inst}}[r,t],$$

$$\Delta S_{\text{inst}}[r,t] = \left(\frac{e^2}{mc^2}\right)^2 P\left\{\left[\sum_{\mu\neq}\sum_\nu \frac{1}{\pi r}\int_0^\infty dr' w_{\mu\nu}(r-r') \times \left(\frac{1}{V(t)} g_{\mu\nu}(r',t) - \frac{1}{V(0)} g^0_{\mu\nu}(r')\right)\right] - \left[\frac{1}{V(t)} - \frac{1}{V(0)}\right]\right\}, \tag{5}$$

$$w_{\mu\nu}(x) = \int_0^\infty dq f_\mu(q) f_\nu(q) \left[\sum_{\mu\neq}\sum_\nu f(q)_\mu f(q)_\nu\right]^{-1} \cos(qx).$$

This expression will now be scrutinized.

B. Physical interpretation of $\Delta S[r,\tau]$

The following characteristics of $\Delta S[r,\tau]$ emerge. (i) The signal $\Delta S_{\text{inst}}[r,t]$ has two terms. The first describes the change in the pair distribution functions $g_{\mu\nu}$ during the chemical reaction, and is thus related to the molecular dynamics of the reactive system. The second-term probes the change in the volume V due to laser heating. (ii) The atom-atom distribution functions $g_{\mu\nu}$ do not enter into $\Delta S_{\text{inst}}[r,t]$ alone, but are coupled with the the atomic form factors f_μ, f_ν, via $w_{\mu\nu}$'s. This blurs the information contained in $\Delta S[r,\tau]$. In spite of this, the following two statements can be made. If the atoms μ,ν belong to different molecules, the corresponding peaks in $\Delta S[r,\tau]$ are mainly shaped by the $g_{\mu\nu}$'s. In contrast, if they are located on the same molecule, the f_μ, f_ν's dominate. (iii) The signal $\Delta S[r,\tau]$ is composed of a number of different $g_{\mu\nu}$'s, but this is not a real handicap. If the bond μ-ν is broken, only the distribution function $g_{\mu\nu}$ of atoms μ,ν forming this bond stands out in the difference signal. Other terms disappear, partially or completely. (iv) Thermal expansion dominates $\Delta S[r,\tau]$ at small r's. At these distances the atoms behave as hard spheres, the $g_{\mu\nu}$'s all vanish and only the term $1/V(t) - 1/V(0)$ survives. As $\Delta V/V = -\Delta\rho_M/\rho_M$, the evolution of the mass density ρ_M of the solvent can be monitored in this region of r.

It results from the above analysis that, although a number of precautions are required, the Fourier transformed signal permits to "film" atomic motions in chemical reactions. The signal $\Delta S[r,\tau]$ is thus appropriate for this type of study, and Eq. (5) permits to monitor the molecular dynamics. However, it should not be forgotten that this conclusion only applies under quasistatic conditions. Equation (2) breaks down if this condition is not satisfied.

C. Atomic liquids

If the liquid is atomic before and after laser excitation, the expression for $\Delta S[r,\tau]$ simplifies considerably. In this case $w_{\mu\nu}(x) = [1/N(N-1)]\pi\delta(x)$, $g_{\mu\nu}(r,t) = g(r,t)$, $g^0_{\mu\nu}(r) = g^0(r)$ for all μ,ν and one finds readily

$$\Delta S[r,\tau] = \int dt I_X(t-\tau)\Delta S[r,t]_{\text{inst}},$$

$$\Delta S_{\text{inst}}[r,t] = \left(\frac{e^2}{mc^2}\right)^2 P\left[\left(\frac{1}{V(t)} g(r,t) - \frac{1}{V(0)} g^0(r)\right) - \left(\frac{1}{V(t)} - \frac{1}{V(0)}\right)\right]. \tag{6}$$

The effect of atomic form factors is eliminated by the above choice of "sharpening factor" $M(q)$. This equation represents a generalization of the familiar Zernicke-Prins formula[27] for time-resolved x-ray experiments. Although the general form of these equations is much the same, two basic differences should be emphasized. (i) The above formula permits the calculation of pair distribution functions as they vary after laser excitation. It thus describes the return of the system to thermal equilibrium, and not a system in thermal equilibrium. The physical content of these two equations is thus very different. (ii) A new term appears in Eq. (6) describing

the effect of thermal expansion. This term, absent in the Zernicke-Prins formula, is present here as it should be. But once again, the similarity between Eq. (6) and the Zernicke-Prins formula disappears completely when one leaves the quasistatic regime.

V. SIMULATIONS AND CALCULATIONS

A. Basic model

The purpose of this section is to show how the above theory was applied to interpret our experiments. Our system contains a single I_2 molecule and a fixed number of CCl_4 molecules in a volume $V(t)$ that varies with time. The reactions $I_2^\star \Rightarrow I_2$ and $I_2^\star \Rightarrow 2I \Rightarrow I_2$ were both supposed to start at time $\tau=0$. The signals $\Delta S(q,\tau)$, $\Delta S[r,\tau]$ were calculated using Eqs. (2) and (5) and the following model: (i) The solution is modeled by a three-level quantum system, representing the electronic states of I_2 perturbed by stochastic solvent-solute interactions. State 1 represents the ground state X, state 2 is its two excited states A, A', and state 3 is a large number of highly excited repulsive states [Fig. 1(b)]. (ii) The processes α, β, and γ are all considered. Vibrational cooling of state 1 (process α), trapping of the two I atoms into state 2 followed by its deexcitation (process β), and escape of I atoms from the solvent cage and their nongeminate recombination (process γ). The first two contribute to geminate and the latter to nongeminate recombination. (iii) The populations of the molecular states 1–3 are taken from spectroscopic data.[7–10,30] One has

$$n_1(\tau) = 1 - n_2(\tau) - n_3(\tau),$$

$$n_2(\tau) = n_2 \exp(-\tau/\tau_\beta),$$

$$n_3(\tau) = n_3 \frac{1}{1 + 2k[\mathrm{I}]_0 \tau},$$

where n_1, n_2, and n_3 are initial populations of the states 1–3, τ_β is the relaxation time of the state A/A', k is the rate constant for nongeminate recombination, and [I] the iodine concentration. The values of n_1, n_2, and n_3 depend on the laser excitation and are supposed to be known.

The above model still needs complementary information. The total diffraction signal $\Delta S(q,\tau)$ is the sum of two terms, $\Delta S(q,\tau) = \Delta S(q,\tau)_\mathrm{I} + \Delta S(q,\tau)_\mathrm{Sol}$. $\Delta S(q,t)_\mathrm{I}$ describes the iodine molecule captured in its cage; the indices μ,ν belong either both to I atoms, or one to I and the second to C or Cl. In turn, the term $\Delta S(q,\tau)_\mathrm{Sol}$ describes the $C-Cl_4$ solvent; the indices μ,ν both belong either to C or Cl. The problem is that if the picosecond and nanosecond time scales are involved in the iodine dynamics, μs times scales intervene in the solvent dynamics. The presence of this long time scale precluded the exclusive use of molecular dynamics, and a recourse to hydrodynamics of continuous media was inevitable. This concession has a high price. Macroscopic hydrodynamics assumes the local thermodynamic equilibrium, which does not exist at times prior to 100 ps. These times are thus excluded from the present study.

TABLE I. Geometrical and potential parameters for the CCl_4 model.

$r_{\mathrm{Cl-Cl}}$	1.769 A
$r_{\mathrm{Cl-Cl}}$	2.890 A
q_C	$0.248e$
q_Cl	$-0.062e$
$\varepsilon_{\mathrm{CC}}$	25.190 K
$\varepsilon_{\mathrm{ClCl}}$	134.010 K
$\varepsilon_{\mathrm{CCl}}$	58.100 K
σ_{CC}	3.800 A
σ_{ClCl}	3.470 A
σ_{CCl}	3.365 A

B. Molecular-dynamics simulation

1. Solvent signals and their derivatives

The static signals $S(q)_\mathrm{Sol}$ of the solvent were calculated by molecular-dynamics simulation. The OPLS pair potential was used to describe liquid tetrachloromethane.[31] In this model, the CCl_4 molecules are considered as rigid tetrahedra, and the pair potentials are atom centered 6–12 Lennard-Jones potentials plus Coulombic potentials from the partial charges on C and Cl. The corresponding parameters are summarized in Table I. The *NVT* simulations were performed with 512 molecules for about 1 ns each, and a time step $\Delta t = 1$ fs was used. Periodic boundary conditions were imposed at all times, as well as Ewald summation of electrostatic terms. The Verlet velocity integrator was employed along with the SHAKE/RATTLE algorithm to keep the solvent rigid.[32] As far as atomic form factors $f_\mu(q)$ are concerned, they were taken from the DABAX database.[33] This procedure leads to good agreement with the experimental $S(q)_\mathrm{Sol}$ for liquid CCl_4 (Fig. 6).

The thermodynamic variables appropriate to the present problem are the temperature T and the density ρ. In order to

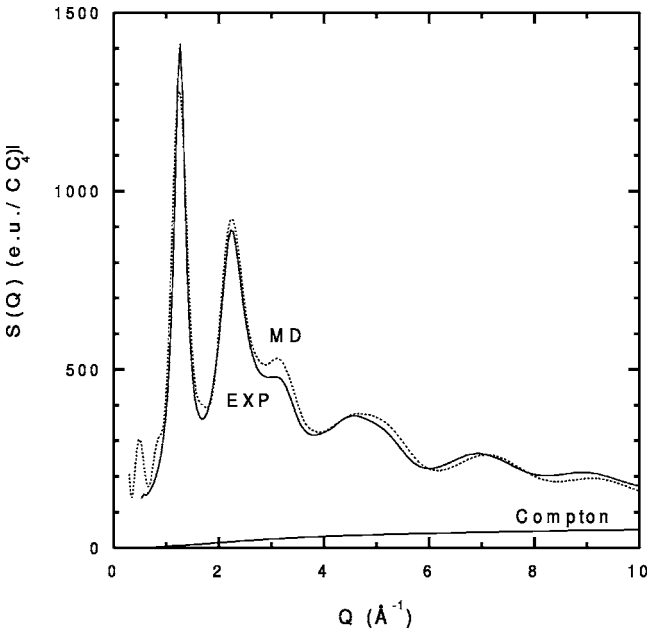

FIG. 6. The x-ray signal $S(q)$ from liquid CCl_4: The solid line corresponds to the experiment, and the dotted curve to the molecular-dynamics simulation with 1024 molecules. The Compton contribution to the signal is also shown (solid line at the bottom).

estimate partial derivatives of the signal $S(q)_{\mathrm{Sol}}$ with respect to these variables, finite differences were used. Two different temperatures were considered, $T_1=300$ K and $T_2=328$ K, and two volumes, $V(T_1)=97.3$ cm^3 and $V(T_2)=100.65$ cm^3. These volumes are molar volumes along the liquid-vapor coexistence curve at T_1 and T_2.[34] Three simulations were run at the thermodynamic points (T_1,V_1), (T_2,V_1), and (T_2,V_2). Then

$$(\partial \Delta S_{\mathrm{Sol}}(q)/\partial T)_V \rightarrow [\Delta S_{\mathrm{Sol}}(q,T_2,V_1) - \Delta S_{\mathrm{Sol}}(q,T_1,V_1)]/(T_2-T_1),$$

$$(\partial \Delta S_{\mathrm{Sol}}(q)/\partial V)_T \rightarrow [\Delta S_{\mathrm{Sol}}(q,T_2,V_2) - \Delta S_{\mathrm{Sol}}(q,T_2,V_1)]/(V_2-V_1).$$

The derivatives with respect to ρ are easily deducible from the derivatives with respect to V as $\rho=N/V$.

2. Iodine signals $\Delta S(q,\tau)_{\mathrm{I}}$

Molecular-dynamics calculations were realized for each electronic state of the iodine molecule, the ground state X, or the excited states A,A', as well as for the free iodine atoms; compare with Eq. (3). The iodine signals $\Delta S(q,\tau)_{\mathrm{I}}$ were defined by the difference of the signal from a system consisting of one excited iodine molecule or atom in 512 CCl_4 molecules minus the signal of a nonexcited solution. The iodine difference signals include not only information about the molecular geometry of the solute, but also about the solvent cage surrounding the molecule or atom. Unfortunately, the cage terms are difficult to determine accurately, and the presence of spurious peaks often complicates the analysis.

In all these simulations, the system was first equilibrated. Ten configurations 10 ps apart were then extracted from a 100 ps long trajectory. In each of them the iodine molecule was stretched from the equilibrium distance to $R=4$ A and the system was allowed to relax toward the equilibrium in microcanonical runs of 100 ps. Small changes in the choice of the initial value of R are irrelevant for the present study. The iodine atoms carried no charge and the interaction with the solvent atoms was described using Lennard-Jones potentials and Lorentz-Berthelot rules. The values $\sigma_{\mathrm{I-I}}=3.8$ A and $\epsilon_{\mathrm{I-I}}=240$ K were taken from Bergsma *et al.*[11] In addition, the variations of the intramolecular I–I distance x were controlled by a Morse potential

$$V(x)=D_e[1-e^{-b(x-x_e)}]^2.$$

The parameters $D_e=12\,547$ cm^{-1}, $b=1.91$ A^{-1}, and $x_e=2.67$ A were taken from Nesbitt and Hynes.[35]

C. Hydrodynamics

The calculation of $\Delta S(q,\tau)_{\mathrm{Sol}}$ was realized as follows:[36] (i) Assuming local thermal equilibrium we wrote

$$\Delta S_{\mathrm{Sol}}(q,\tau)=(\partial \Delta S_{\mathrm{Sol}}(q)/\partial T)_\rho \Delta T(\tau) + (\partial \Delta S_{\mathrm{Sol}}(q)/\partial \rho)_T \Delta\rho(\tau), \quad (7)$$

where $\Delta T(\tau)$, $\Delta\rho(\tau)$ are deviations of the temperature and density from their equilibrium values T,ρ. (ii) Once thermodynamic derivatives were determined as described, the temperature and density increments $\Delta T(\tau)$ and $\Delta\rho(\tau)$ remained to be calculated. This can be done using hydrodynamics of continuous media.[37] (iii) The I_2/CCl_4 solution was assumed to be an inviscid fluid. The incoming laser beam delimits a cylinder, the bases of which are equal to the laser beam cross section, and its length to the diameter of the liquid jet (Fig. 7). The distribution of the laser intensity across the beam cross section was supposed to be Gaussian. The absorbed energy, initially contained in excited iodine molecules, spreads after relaxation into their surroundings and heats the solvent. Irregular hydrodynamic effects appear at short times, which gradually transform into a sound wave outside of the laser-illuminated volume. (iv) The laser-induced temperature and density increments were determined using equations of hydrodynamics for inviscid fluids. Under the conditions of our experiment, the equations can be linearized. Then, denoting by $T'(t)$, $\rho'(t)$ the temperature and density increments $\Delta T(t)$, $\Delta\rho(t)$, the following equations can be used

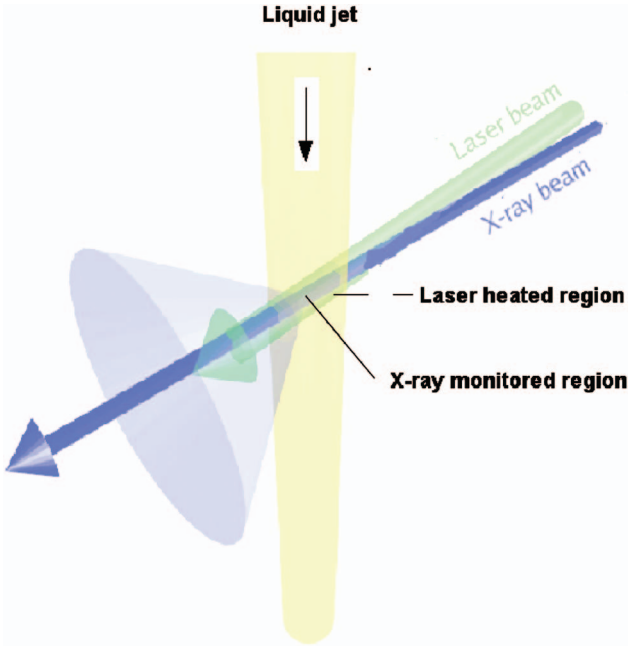

FIG. 7. (Color) Relative orientations of the laser beam, the x-ray beam and the liquid jet.

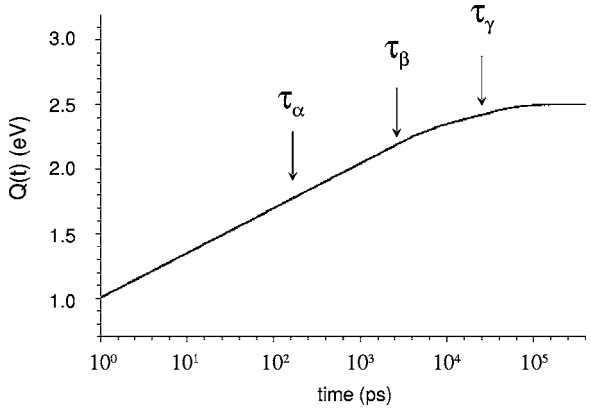

FIG. 8. Temporal variation of the energy density $Q(t)$ injected into the solution. It follows the rhythm of the relaxation processes α, β, and γ. The relaxation times τ_α, τ_β, and τ_γ are indicated by arrows.

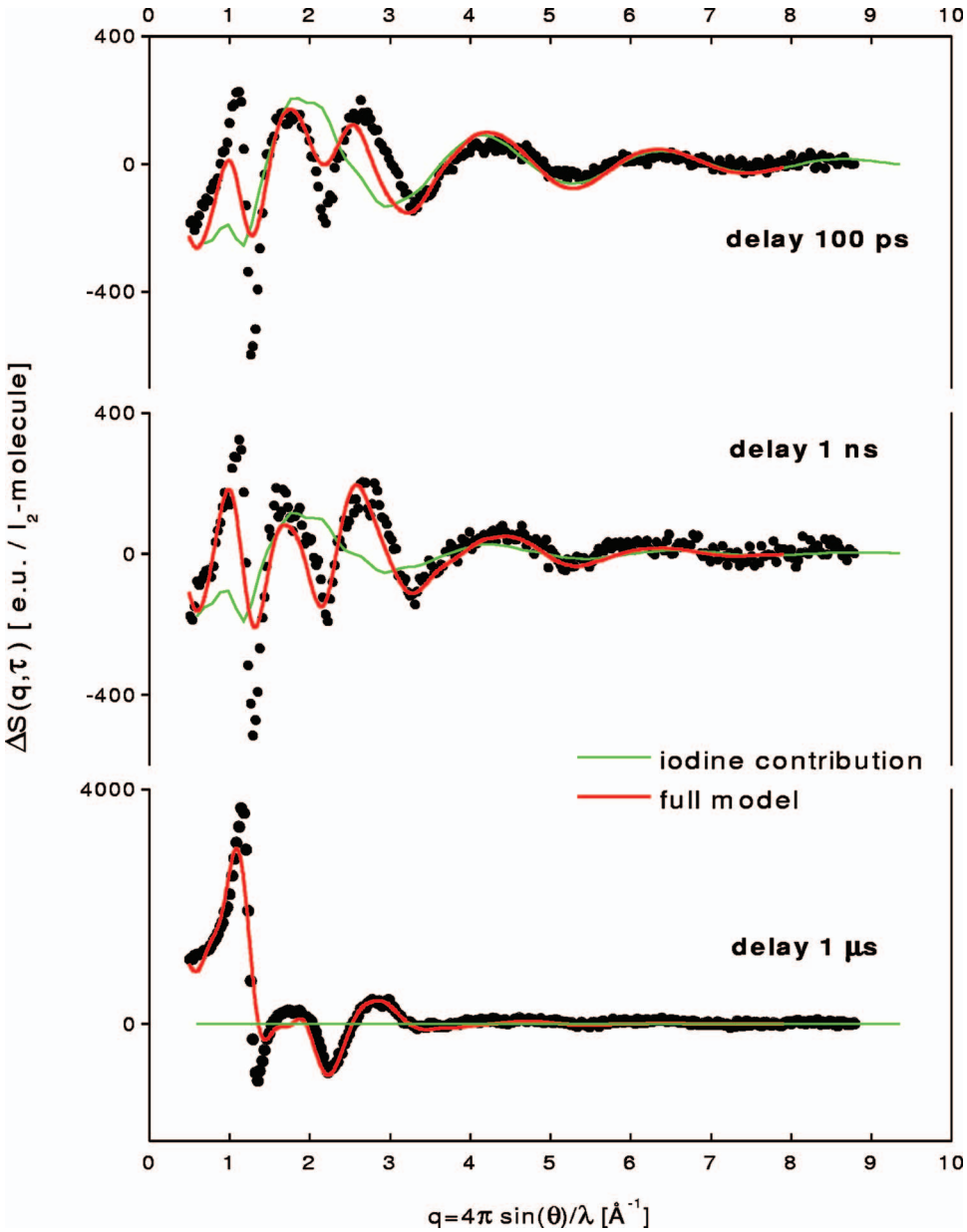

FIG. 9. (Color) The q-resolved scans $\Delta S(q,\tau)$ for the time delays 100 ps, 1 ns, and 1 μs. The circles represent experimental data, red curves the full model, and green curves the iodine contribution.

to calculate the time-dependent parts of $T'(t)$, $\rho'(t)$ (Ref. 37).

$$\nabla^2\rho' - \frac{1}{c}\frac{\partial^2\rho'}{\partial t^2} = \frac{\alpha_p}{C_p}\nabla^2 Q, \tag{8}$$

$$T' = \frac{Q}{C_\nu\rho_0} + \frac{C_p - C_\nu}{C_\nu}\frac{1}{\alpha_p\rho_0}\rho'. \tag{9}$$

Here $Q(t)$ denotes the heat input per unit volume accumulated up to the time t, C_p is the specific heat per unit mass at constant pressure, C_ν the specific heat per unit mass at constant volume, c the sound velocity, α_p the coefficient of isobaric thermal expansion, and ρ_0 the equilibrium density. (v) The heat input $Q(\tau)$, i.e., the laser energy absorbed and released per unit volume by the iodine molecules, follows the rhythm of the different relaxation processes (Fig. 8). The first rise in $Q(\tau)$ corresponds to the passage from the laser excited I_2 to the hot molecule $I_2^\star$. As this process evolves on the picosecond time scale, it appears as a vertical jump at time zero. Further rise corresponds to geminate the recombination of I_2 in 180 ps. Other contributions are associated with the relaxation of the A/A' states in 2.7 ns, and with nongeminate recombination occurring in about 25 ns. (vi) While the expression for $T'(\tau)$ is obtained immediately from $Q(\tau), \rho'(\tau)$, the calculation of $\rho'(\tau)$ is not trivial. An approximate solution, valid perpendicular to the axis of the cylinder, was found by Longaker and Litvak.[38] Slightly extended in the present work, it has the following form:

$$\rho'(\tau) = \frac{\alpha_p}{C_p}\int_{-\infty}^{\tau} dt\left(\frac{dQ(t)}{dt}\right)[-1 + \exp(-c^2(\tau - t)^2/R^2)], \tag{10}$$

where R is the radius of the laser spot. The important feature of the Longaker-Litvak solution is that the thermal expansion does not set in immediately after the heat input, but is delayed as perturbations in a liquid cannot propagate faster than sound waves. There exists an acoustic horizon; the quantity $R/c = \tau_a$ is often called the acoustic transit time. Us-

ing a solution valid perpendicular to the axis of the laser-illuminated cylinder is not a heavy handicap. The axis of the x-ray-defined cylinder is not collinear with it and its basis is smaller than the laser spot. Once $\Delta\rho(\tau)$, $\Delta T(\tau)$ are known, the pressure increment $\Delta p(\tau)$ can be calculated using the thermodynamic expression

$$\Delta p = (1/\rho\chi_T)\Delta\rho + (\alpha_p/\chi_T)\Delta T,$$

where χ_T denotes the isothermic compressibility.

VI. RESULTS AND DISCUSSION

A. General outline

Three sorts of scans will be examined below. In q-resolved scans the signal $\Delta S(q,\tau)$ is considered as a function of q, whereas τ is kept constant. In τ-resolved scans the signal $\Delta S(q,\tau)$ is considered as a function of τ, whereas q is kept constant. Finally, the Fourier-transformed signal $\Delta S[r,\tau]$ also merits discussion. Each of these scans provides unique information, and it is preferable to study them together. There are many similarities and many differences between the time-resolved x-ray scans and time-resolved optical spectra. They will be discussed below in order to facilitate the comparison of these two techniques.

Before interpreting the experimental data, an unexpected finding should be mentioned. Given that only iodine molecules are initially excited, one would expect the solvent signal to stay more or less constant and therefore $\Delta S(q,\tau)_{\mathrm{Sol}}$ to be small or even very small. This is not the case, the energy released by excited molecules heats the solvent and initiates its structural rearrangement and thermal expansion. The signature of this process is unexpectedly large since it involves all CCl_4 molecules in the x-ray-illuminated volume. The contribution of the solvent to the signal $\Delta S(q,\tau)$ was found to be comparable to that of iodine.

B. Signals $\Delta S(q,\tau)$

The q-resolved scans are examined first with τ kept constant (Fig. 9). We note that the information content depends on the q range. (i) In the high q range, $4.3<q<8.8$ A^{-1}, the "naked" iodine structures are seen as they relax progressively towards the ground state. This statement is confirmed by the presence of oscillations similar to those expected from gas-phase iodine. Their temporal evolution agrees with the data from optical spectroscopy. (ii) By contrast, in the low q range $0.5<q<4.3$ A^{-1}, the thermal expansion of CCl_4, heated by relaxing iodine molecules, is observed. To check this conjecture, the difference signal $\Delta S(q,\tau)_{\mathrm{Sol}}$ was calculated as described earlier. We found good agreement between theory and experiment which strongly supports the above conjecture. Another argument in favor of this interpretation is that a similar behavior was found in many other systems such as I_2/CH_2Cl_2, I_2/CH_3OH, etc.

The τ-resolved scans are studied next. It should be kept in mind that fixing the length q of the wave vector defines the length scale $l\sim 1/q$ of the molecular process under investigation. As these take place at different length scales, the τ-resolved scans should depend significantly on the choice of q (Fig. 10). (i) If $q<4.3$ A^{-1}, the signal $\Delta S(q,\tau)$ increases with time. It probes thermal expansion of the laser-heated liquid. We expect this behavior to be quite general; heating a system generates necessarily thermal expansion. (ii) When $q=4.3$ A^{-1}, the signal $\Delta S(q,\tau)$ decreases with time: it probes the relaxation of the excited iodine molecules and the recombination of iodine atoms. The "asymmetry" in the time dependence of the signals is thus explained in a natural way. It is interesting to note that, according to the present theory, only 14% of laser-excited iodine molecules escape the solvent cage.

The similarity between the above analysis of q- and τ-resolved x-ray scans and that currently employed in optical spectroscopy is worth noting. The q-resolved x-ray scans are analogous to the frequency-resolved optical spectra, and τ-resolved x-ray scans are similar to the time-resolved optical spectra. The difference is that in x-ray scans different processes may dominate at different distances $r\sim 1/q$, whereas in optical spectra different processes are followed at different energies E. The rest of the analysis is similar.

C. Fourier-transformed signal $\Delta S[r,\tau]$

The Fourier-transformed diffraction signals $\Delta S[r,\tau]$ are shown in Fig. 11. Experimental points were obtained by numerical integration of the measured signals $\Delta S(q,\tau)$. This integration extended over the variable q, and was performed for different values of r. Theoretical values were obtained using Eq. (5) directly, without recourse to the experiment. The chosen time delays were $\tau=200$ ps, 1 ns, and 1 μs.

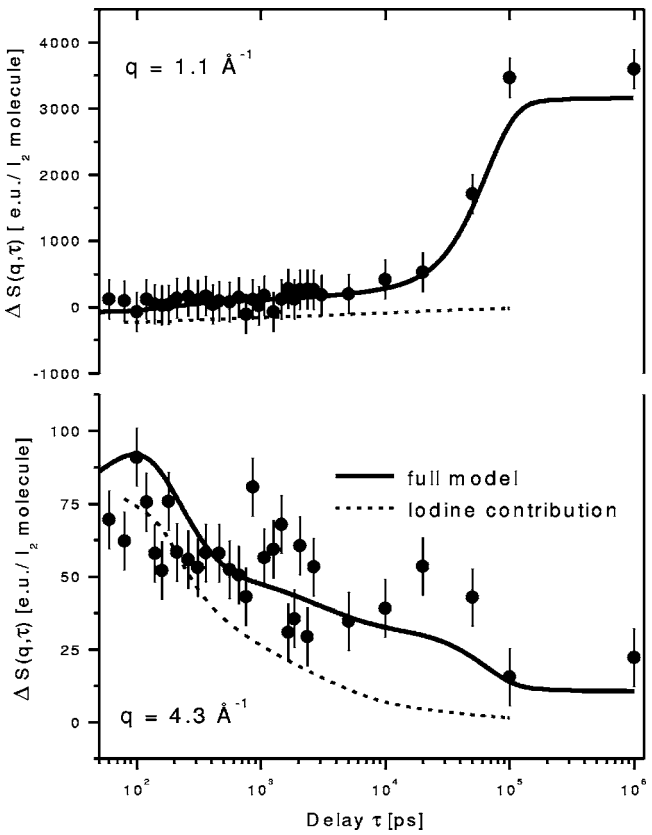

FIG. 10. The τ-resolved scans $\Delta S(q,\tau)$ at $q=1.1$ A^{-1} and $q=4.3$ A^{-1}. The circles represent experimental data, solid lines the full model, and dashed lines the iodine contribution.

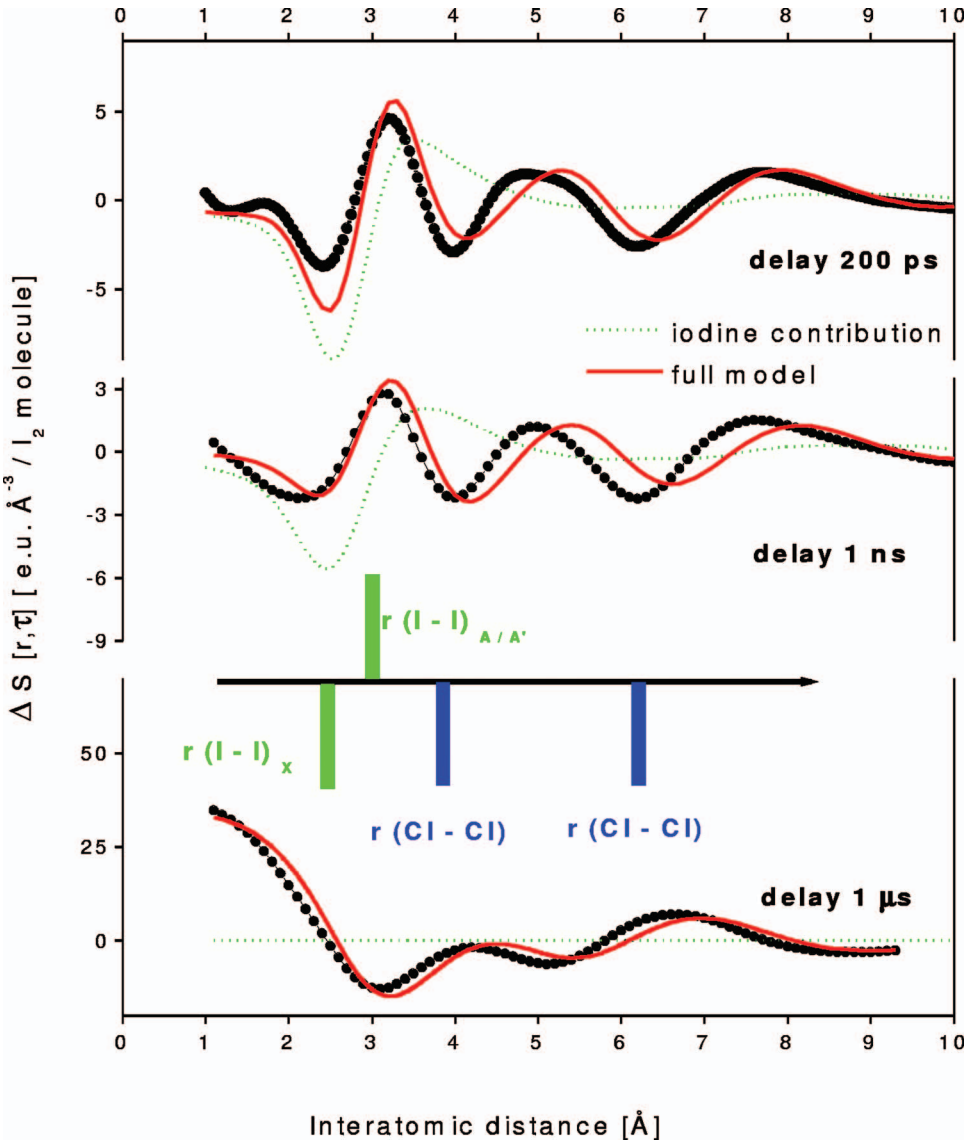

FIG. 11. (Color) The Fourier-transformed signals $\Delta S(r,\tau)$ for the time delays 200 ps, 1 ns, and 1 μs. The green bars indicate the bond lengths of I_2 in the X and A/A' states, and the blue bars illustrate the positions of the first two peaks of g_{Cl-Cl}.

They should be compared to the relaxation times $\tau_\alpha = 0.18$ ns, $\tau_\beta = 2.7$ ns, and $\tau_\gamma = 25$ ns of the system. The following interpretation of Fig. 11 may be proposed.

(i) The first minimum observed at 2.7 A at early times is due to the depletion of the X state of the molecular iodine from the laser excitation. The excited molecules reach the A/A' and higher electronic states, and a maximum appears around 3.2 A. As molecules having left the ground state X are those excited, the negative peak at 2.7 A and the positive peak at 3.2 A should have roughly similar area, which is indeed observed. (ii) The energy transfer from the solute molecule to the solvent gives rise to a structural rearrangement of the latter. New peaks in $\Delta S[r,\tau]$ thus appear. Our molecular-dynamics simulations showed that the new minima at 4.0 and 6.2 A are mainly due to the changes in intermolecular Cl–Cl distances in CCl_4. In fact, the atomic pairs I–C and I–Cl are difficult to detect in diluted solutions, the quantities w_{I-C}, w_{I-Cl}, and w_{CCl} are too small. (iii) At later times, where $\tau \gg \tau_\alpha$, $\tau \gg \tau_\beta$, and $\tau \gg \tau_\gamma$, the excited states of I_2 have all relaxed. The features observed at large r's then reflect the variations in the intermolecular Cl,…,Cl distances upon heating. In turn, the strong increase of $\Delta S[r,\tau]$ "seen" at small r's is due to the decrease in the mass density ρ_M of CCl_4. Time-resolved x-ray diffraction thus permits the detection of temporally varying the I–I atom-atom distribution functions. Simultaneous changes in the structure of the CCl_4 solvent are monitored too: the solvent appears as a reaction partner rather than an inert medium.[39]

Moreover, this technique also permits to follow temporal variations of thermodynamic quantities such as $\Delta\rho(t)$, $\Delta T(t)$, and $\Delta p(t)$ after laser excitation. One just has to extract $\Delta\rho(t)$ from the small-r portion of the measured $\Delta S[r,\tau]$, and to deduce $\Delta T(t)$, $\Delta p(t)$ via the thermodynamic relations given earlier. Real-time plots of $\rho(t)$, $T(t)$, and $p(t)$ obtained in this way are shown in Fig. 12. Moreover, the thermodynamic evolution of the laser-heated system is illustrated in Fig. 13. The influence of the acoustic transit time, retarding the structural evolution by the presence of the acoustic horizon, is clearly visible: the mass density $\rho_M(\tau)$ remains constant up to times of the order of 10 ns. How does this delay influence chemical reaction rates? This question has not yet been investigated.

The present discussion may be closed by noticing that if

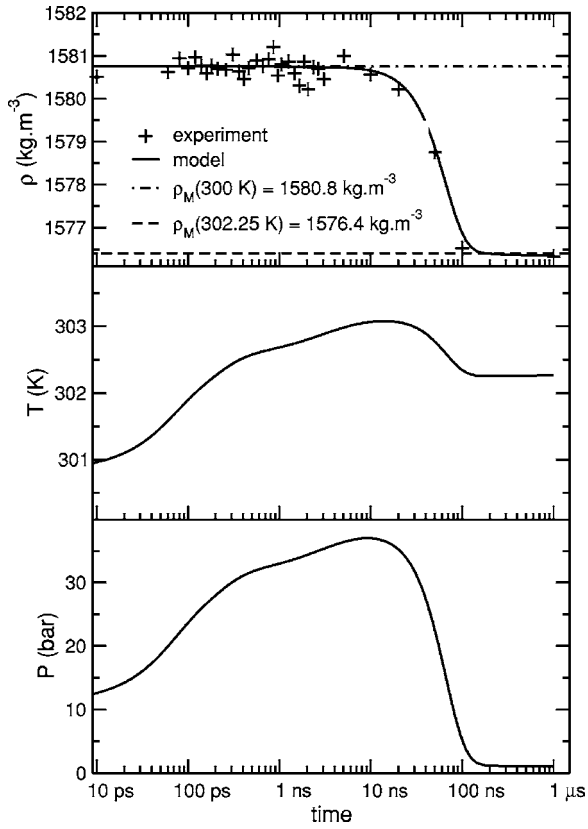

FIG. 12. Temporal variations of $\Delta\rho(t)$, $\Delta T(t)$, and $\Delta p(t)$ after laser excitation. The delay in $\rho_M(t)$ due to the acoustic horizon is easily seen.

$\Delta S(q,\tau)$ scans resemble time-resolved optical spectra to some extent, this similarity is completely lost for the Fourier-transformed signal $\Delta S[r,\tau]$. This signal simply has no optical analogue: the optical wave length λ is large compared to intermolecular distances l. The above discussion illustrates the advantage of x-ray monitoring of atomic motions as compared to optical monitoring. Single atom motions can in principle be visualized by the former technique, but only motions averaged over the pump-prepared wave packet are detectable by the latter.

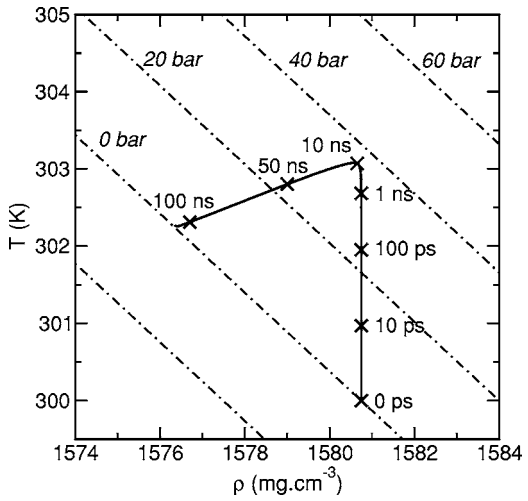

FIG. 13. Thermodynamic evolution of a laser heated system.

VII. CONCLUSIONS

Time-resolved x-ray-diffraction techniques have made considerable progress over the last five years. Advances in source technology have driven a wide variety of experiments using both synchrotrons and small laboratory-based systems. The theory has advanced considerably too. It has many points in common with that of time-resolved optical spectroscopy. It is now possible to follow transient structures during the course of various photophysical, chemical and biological processes. Moreover, x-ray-diffraction techniques also permit to monitor structural changes of the solvent during a chemical reaction. One concludes that a hundred years after Roentgen's fundamental discovery, real-time "filming" of atomic motions in liquids has become reality.

ACKNOWLEDGMENTS

The authors would like to thank P. Anfinrud, F. Schotte, R. Neutze, J. Davidson, W. Reichenbach, L. Eybert, L. Claustre, G. Naylor, Y. Petroff, and J-Cl Leicknam for their help during this work as well as for many useful suggestions. One of the authors (H.I.) also acknowledges the support by the Korea Research Foundation Grant founded by the Korean Government (MOEHRD, R08-2004-000-10076-0).

[1] J. Franck and E. Rabinowitch, Trans. Faraday Soc. **30**, 120 (1934).
[2] E. Rabinowitch and W. C. Wood, Trans. Faraday Soc. **32**, 547 (1936).
[3] E. Rabinowitch and W. C. Wood, Trans. Faraday Soc. **32**, 1381 (1936).
[4] J. Zimmerman and R. M. Noyes, J. Chem. Phys. **18**, 658 (1950).
[5] F. W. Lampe and R. M. Noyes, J. Am. Chem. Soc. **76**, 2140 (1954).
[6] R. Mulliken, J. Chem. Phys. **55**, 288 (1971).
[7] T. J. Chuang, G. W. Hoffman, and K. B. Eisenthal, Chem. Phys. Lett. **25**, 201 (1974).
[8] A. L. Harris, M. Berg, and C. B. Harris, J. Chem. Phys. **84**, 788 (1986).
[9] N. A. Abul-Hai and D. F. Kelley, J. Chem. Phys. **84**, 1335 (1986).
[10] A. L. Harris, J. K. Brown, and C. B. Harris, Annu. Rev. Phys. Chem. **39**, 341 (1988).
[11] J. P. Bergsma, M. H. Coladonato, P. M. Edelstein, J. D. Kahn, K. R. Wilson, and D. R. Fredkin, J. Chem. Phys. **84**, 6151 (1986).
[12] D. A. Reis, M. F. DeCamp, P. H. Bucksbaum *et al.*, Phys. Rev. Lett. **86**, 3072 (2001).
[13] A. Rousse, C. Rischel, S. Fourmaux *et al.*, Nature (London) **410**, 65 (2001).
[14] B. Perman, V. Srajer, Z. Ren *et al.*, Science **279**, 1946 (1998).
[15] S. Techert, F. Schotte, and M. Wulff, Phys. Rev. Lett. **86**, 2030 (2001).
[16] F. Schotte, M. Lim, T. A. Jackson, A. V. Smirnov, J. Soman, J. Olson, G. N. Phillips, M. Wulff, and P. A. Anfinrud, Science **300**, 1944 (2003).
[17] L. X. Chen, W. J. H. Jaeger, G. Jennings, D. J. Goszotola, A. Munkholm, and J. P. Hessler, Science **292**, 262 (2001).
[18] M. Saes, C. Bressler, R. Abela, D. Grolimund, S. L. Johnson, P. A. Heimann, and M. Chergui, Phys. Rev. Lett. **90**, 047403 (2003).
[19] R. Neutze, R. Wouts, S. Techert, J. Davidson, M. Kocsis, A. Kirrander, F. Schotte, and M. Wulff, Phys. Rev. Lett. **87**, 195508 (2001).
[20] M. Ben-Nun, J. Cao, and K. R. Wilson, J. Phys. Chem. A **101**, 8743 (1997).
[21] S. Bratos, F. Mirloup, R. Vuilleumier, and M. Wulff, J. Chem. Phys. **116**, 10605 (2002).
[22] A. Plech, M. Wulff, S. Bratos, F. Mirloup, R. Vuilleumier, F. Schotte, and Ph. A. Anfinrud, Phys. Rev. Lett. **92**, 125505 (2004).
[23] S. Bratos, F. Mirloup, R. Vuilleumier, M. Wulff, and A. Plech, Chem. Phys. **304**, 245 (2004).
[24] F. Schotte, S. Techert, P. Anfinrud, V. Srajer, K. Moffat, and M. Wulff, *Third Generation Hard X-Ray Synchrotron Radiation Sources: Source Properties, Optics, and Experimental Techniques* (Wiley, New York, 2002).
[25] A. Plech, R. Randler, A. Geis, and M. Wulff, J. Synchrotron Radiat. **9**, 287 (2002).
[26] A. P. Hammersley, S. O. Svensson, M. Hanfland, A. Fitch, and D.

Hausermann, High Press. Res. **14**, 235 (1996).
[27] B. E. Warren, *X-Ray Diffraction* (Dover, New York, 1969).
[28] J. Als-Nielsen and D. McMorrow, *Elements of Modern X-Ray Physics* (Wiley, New York, 2001).
[29] A. H. Narten and H. A. Levy, Science **165**, 447 (1969).
[30] R. Marchall and N. Davidson, J. Chem. Phys. **21**, 2086 (1953).
[31] E. M. Duffy, D. L. Severance, and W. L. Jorgensen, J. Am. Chem. Soc. **114**, 7535 (1992).
[32] J. P. Ryckaert, G. Ciccotti, and H. J. C. Berendsen, J. Comput. Phys. **23**, 327 (1977).
[33] http://www.esrf.computing/scientific/dabax
[34] D. R. Lide and H. V. Kehiaian, *CRC Handbook of Thermophysical and Thermochemical Data* (CRC, Boca Raton, FL, 1994), p. 81.
[35] D. J. Nesbitt and J. T. Hynes, J. Chem. Phys. **77**, 2130 (1982).
[36] F. Mirloup, R. Vuilleumier, S. Bratos, M. Wulff, and A. Plech, in *Femtochemistry and Femtobiology*, edited by M. Martin and J. T. Hynes (Elsevier, Amsterdam, 2004), p. 349.
[37] L. D. Landau and E. M. Lifshitz, *Course of Theoretical Physics:Fluid Mechanics* (Pergamon, London, 1959), Vol. 6.
[38] P. R. Longaker and M. M. Litvak, J. Appl. Phys. **40**, 4033 (1969).
[39] A. Rice, Nature (London) **429**, 255 (2004).